# University of Essex

# Research Repository

## Motion stability analysis of beaver-like robot

Research Repository link: https://repository.essex.ac.uk/40121/

**Please note:**

www.essex.ac.uk

# Motion stability analysis of beaver-like robot

Gang Chen[1,2,3,4]  Y i d o n g X u [1], Zhenyu Wang[1], Huosheng Hu[2] and Chuanyu Wu[1,5]

## Abstract

A stability index and evaluation method based on couple moment judgment are proposed for the motion stability of beaver-like robot. The index, expressed by the ratio of the recovery torque and external disturbance torque caused by gravity and buoyancy of the beaver-like robot, effectively evaluates the robot's motion stability. The swimming stability index of beaver-like robot is calculated on the basis of Adams–Matlab co-simulation. Through comparative analysis of the indexes calculated in accordance with experimental and simulation data under different gaits, the stability of the robot in the rolling direction is confirmed to be worse under alternating gaits. The stability in the pitching direction is worse under synchronous gaits. Moreover, the increase of the motion amplitude of the propulsion structure (hind legs and tail) reduces the motion stability of the robot. This research can lay the foundation for stability criteria in underwater stable motion control and motion optimization of beaver-like robots.

## Introduction

With the increasing demand for ocean exploration, the continuous development of underwater robot technology provides strong support for marine scientific research and engineering applications.[1,2] As a design concept inspired by nature,[3–5] bionic underwater robots have shown great potential in the fields of ocean exploration, resource exploration, and environmental monitoring.[6–8] The beaver is an amphibian with excellent swimming ability and motion stability; as such, it serves as an important reference for the design of bionic underwater robots.[9] Learning from the biological characteristics and behaviors of beavers can further improve the performance and adaptability of bionic underwater robots in the marine field. The wide application of these robots in marine science and engineering can also be promoted.[10,11]

Our team used the beaver as the biomimetic object to carry out many studies on robot design, motion control, and hydrodynamic analysis.[12,13] In our study of robot motion control, we found that the dynamic complexity of the underwater environment has strict requirements for the motion control of the bionic underwater robot.[14] Among them, robot stability analysis is crucial for improving the motion control performance of robots, including stability identification,[15] control system design,[16] and stability simulation.[17] Since the 1950s, robot stability analysis has received growing attention, leading to numerous research findings.[18,19] For example, Mejri et al. studied the dynamic characteristics and stability of processing robots to improve the processing quality.[20] Seo et al. designed a wall-climbing robot and completed its stability analysis to improve the robot's motion performance.[21] Zake et al. proposed a stability analysis method of cable-driven parallel robot on the basis of vision control, which can effectively analyze the motion stability of the robot.[22] Liljeback et al. studied the

[1]School of Mechanical Engineering, Zhejiang Sci-Tech University, Hangzhou, Zhejiang, China
[2]School of Computer Science and Electronic Engineering, University of Essex, Colchester, UK
[3]Donghai Laboratory, Zhoushan, Zhejiang, China
[4]Zhejiang Marine Intelligent Ship Institute, Hangzhou, Zhejiang, China
[5]Zhejiang Ocean University, Zhoushan, Zhejiang, China

motion stability of a planar snake robot and proved that the control law of asymptotic stability of a planar snake robot to the equilibrium point must be time varying.[23] Wen et al. studied the stability of the position and force control of the robot arm to increase accuracy of the control.[24] Liang et al. studied the design and stability of wall-climbing robot on the basis of the propeller propulsion force and analyzed the stability conditions of robot adsorbed on the wall.[25] The above research demonstrates the important role of stability analysis in improving the motion performance and motion adaptability of robots.

There have been many methods for stability analysis such as angular momentum measure,[26] force-angular stability measure,[27] energy stability margin measure,[28] Poincare-Lyapunov theory,[29] etc. However, the beaver-like robot is a kind of underwater bionic robot, and its design is inspired by the biological characteristics of the beaver. The robot has complex mechanical structure and dynamic characteristics, and its motion pattern is also significantly different from that of conventional robots.[30] Because its swimming mode is not pure rotational motion, the dynamic model is usually nonlinear and there is no clear equilibrium point in the swimming process, which involves complex hydrodynamic effects and energy conversion process.[31–33] The existing methods are not directly applicable to the stability analysis of the beaver-like robot. Therefore, this study investigates the motion stability of the beaver-like robot, and its main contributions are as follows:

1. We propose a stability index and evaluation method on the basis of the determination of the couple moment for the motion of the beaver-like robot. The index, expressed by the ratio of the recovery torque formed by gravity and buoyancy to the external disturbance torque, effectively evaluates the motion stability of the beaver-like robot.
2. The swimming stability index of the beaver-like robot is calculated on the basis of the Adams-Matlab co-simulation. The stability index is calculated and compared using the experimental and simulation data under different gaits. The stability

of the robot motion under different gaits is obtained, which lays the foundation for the underwater motion control and motion optimization of the beaver-like robot.

The structure of this paper is as follows: Section "Design of beaver-like robot" introduces the structure and gait of the beaver-like robot. Section "Stability index and evaluation method of beaver-like robot" proposes the swimming stability index and evaluation method of the beaver-like robot. Section "Simulation and experiment of swimming stability criteria for beaver-like robot" presents the simulation and experimental study of the swimming stability criteria of the beaver-like robot. Section "Conclusions and future work" discusses the findings and concludes.

## Design of beaver-like robot

A beaver is a semi-aquatic animal,[34] with developed hind legs and a flat tail, enabling it to swim flexibly in water.[35] The biological structure of a beaver is shown in Figure 1(a), featuring long and powerful hind legs with webbed soles to provide large thrust. The broad and flat tail of beavers also provides thrust while maintaining body balance.[36,37] As shown in Figure 1(b), the structure of the beaver-like robot is designed to mimic the body structure of the beaver. Table 1 shows the structural parameters of each part of the robot. Its hind legs have flexible webbed hind feet. The hind legs of the beaver-like robot adopt a two-link articulated structure, including the thigh, shank, and flipper. These components are connected by the hip, knee, and ankle joints.

As shown in Figure 2, the coordinated movement of a beaver's legs under water presents different patterns. Two swimming gaits of beavers have been analyzed so far. In the alternating gait, when the beaver is relaxed, its hind legs alternate in the water, smoothly sliding forward. By contrast, in the synchronous gait, when the beaver needs to accelerate, its hind limbs stroke at the same frequency, producing a high-speed thrust. This study on the stability of the beaver-like robot focuses on these two gaits.
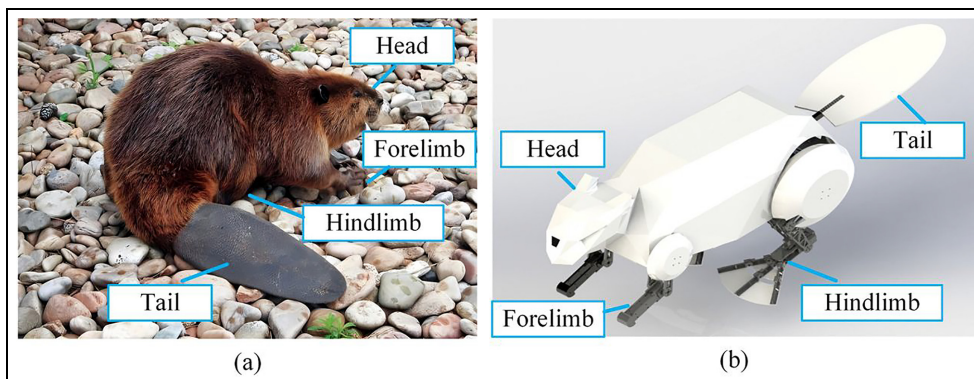


**Figure 1.** Structure of (a) biological beaver and (b) beaver-like robot.
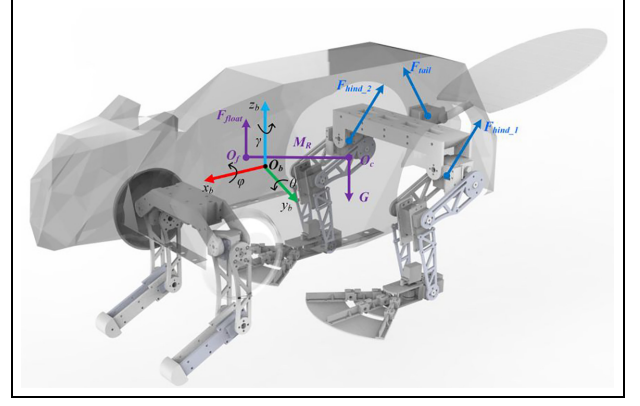
**Table 1.** Parameters of the robot.

| Parts | Parameters | Numerical value |
|---|---|---|
| Body | Overall length (mm) | 700 |
| | Weight (kg) | 5.32 |
| Forelimb | Forearm length (mm) | 100 |
| | Large arm length (mm) | 100 |
| Hindlimb | Shank length (mm) | 122 |
| | Thigh length (mm) | 100 |
| Flipper | First finger length (mm) | 30 |
| | Second finger length (mm) | 50 |
| | Fully extended area (mm$^2$) | 10,353 |
| Tail | Length (mm) | 23 |
| | Area (mm$^2$) | 18,431 |



**Figure 3.** Schematic of the forces acting on beaver-like robot.

## Stability index and evaluation method of beaver-like robot

The motion stability of the beaver-like robot can be quantified by the ratio of the disturbance torque and recovery torque. The couple moments generated by gravity and buoyancy in the recovery torque are related to the positions of the centers of gravity and buoyancy. Owing to the movement of the hind legs and tail of the beaver-like robot, the centers of gravity and buoyancy change with the robot's attitude, so a model with varying centers of buoyancy and gravity is established. The interference torque includes the interference force generated by the hind legs and tail and the water resistance of the robot's overall shell.

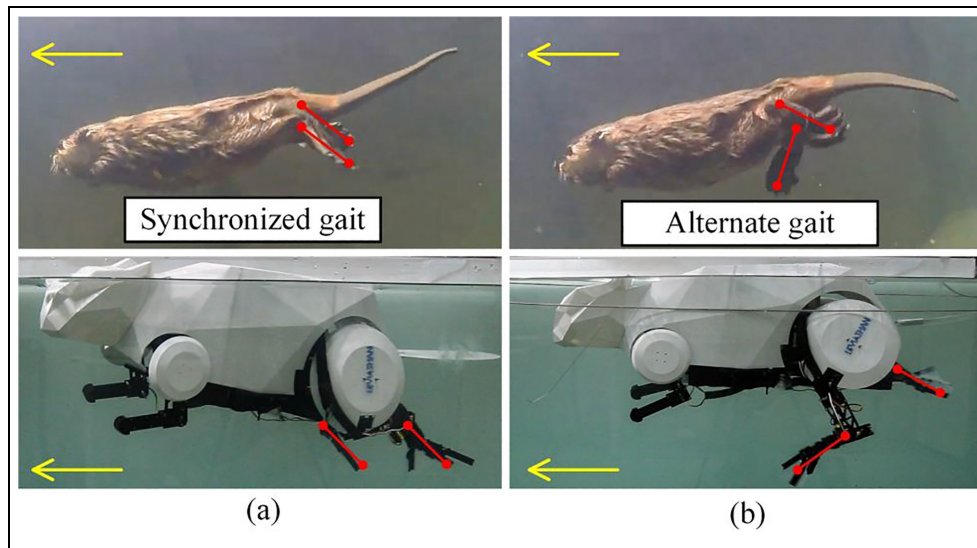### Stability index of beaver-like robot

As shown in Figure 3, the robot body coordinate system $o_b x_b y_b z_b$ is firmly connected with the body. The body rotates following the right-hand spiral direction. The angle of rotation around the $o_b x_b$ axis is the roll angle $\phi$ (roll), that around the $o_b y_b$ axis is the pitch

angle $\theta$ (pitch), and that around the $o_b z_b$ axis is the yaw angle $\gamma$ (yaw).

The gravity and buoyancy forces acting on the robot forms a couple, generating a couple moment (as shown in Figure 3). This moment, called the recovery moment $M_R$, counteracts the robot's rolling or pitching caused by other environmental forces (interference moment $M_D$). The direction of the recovery moment opposes that of roll and pitch, inhibiting the latter's growth. When the interference moment is smaller than the recovery moment, the robot's attitude change can be suppressed, so the robot can swim stably. On the contrary, an imbalance can cause unstable swimming. In this study, the ratio $M_D/M_R$ between the disturbance torque $M_D$ and the recovery torque $M_R$ is used as the discriminant index for robot swimming stability. A ratio of $M_D/M_R < 1$ means stable swimming; $M_D/M_R = 1$, metastable swimming; $M_D/M_R > 1$, unstable swimming.

The change in attitude angle can be used to describe the motion change of the beaver-like robot while swimming under water. However, the dynamic stability of



**Figure 2.** Kinematic gaits: (a) synchronous gait, (b) alternating gait.

the beaver-like robot cannot be evaluated only from the change of attitude angle. The stability index based on the determination of the couple moment can better describe the stability of the robot during dynamic motion. This index not only considers the stability under static conditions, but also implies the recovery ability in the dynamic process, because the recovery torque is often closely related to the dynamic characteristics of the robot, such as mass distribution, propulsion mode, etc. This dynamic adaptability makes the metric more advantageous when evaluating robot stability in complex underwater environments.

## Calculation of swimming stability index of beaver-like robot

The propulsion mechanism of the beaver-like robot during swimming mainly involves its hind legs and tail. Our previous research has focused on the dynamics of the hind legs and tail. We thus proposed a rigid-liquid fusion dynamics model combining robot rigid body dynamics and hydrodynamics [0] and a segmented dynamics model integrating the deflection deformation principle and hydrodynamics of the tail.[38] These models have been verified by theoretical model calculation, simulation, and experiment. The theoretical, experimental, and simulation values for the hydrodynamic forces exerted by the hind legs $F_h$ and the tail $F_t$ are obtained.

The disturbance torque $M_D$ of the beaver-like robot is composed of the hydrodynamic force of the hind legs $F_h$, tail $F_t$, and shell $F_s$. It can be expressed as follows:

$$M_D = F_h \cdot s_h + F_t \cdot s_t + F_s \cdot s_m$$
$$= \begin{bmatrix} F_{h\_x} \cdot x_h + F_{t\_x} \cdot x_t + F_{s\_x} \cdot x_m \\ F_{h\_y} \cdot y_h + F_{t\_y} \cdot y_t + F_{s\_y} \cdot y_m \\ F_{h\_z} \cdot z_h + F_{t\_z} \cdot z_t + F_{s\_z} \cdot z_m \end{bmatrix} = \begin{bmatrix} M_{D\_\varphi} \\ M_{D\_\theta} \\ M_{D\_\gamma} \end{bmatrix}$$

(1)

Where $s_h$, $s_t$, and $s_m$ are the coordinates of the hind leg hip joint, the tail joint, and the robot's centroid in the body coordinate system, respectively. The hydrodynamic force of the hind leg $F_h$ is calculated using the hydrodynamic model of the hind leg of the beaver-like robot, which is equivalent to the force acting on the hip joint of the beaver-like robot. The hydrodynamic force of the tail $F_t$ is calculated using the water-saving dynamic model of the tail part of the beaver-like robot, which is equivalent to the force acting on the tail joint of the beaver-like robot. The hydrodynamic force of the shell $F_s$ is the resistance of the whole robot against the water flow while swimming, which is obtained by simulating of the underwater motion of the robot using ANSYS Fluent simulation software. It is equivalent to the force acting on the center of mass of the robot. The simulation of the shell in ANSYS Fluent is shown in Figure 4, where the fluid simulation of the shell is performed in a steady-state mode. The left side is the fluid velocity inlet, with velocities ranging from 0 increasing by 0.1 to 1 m/s. The right side is the pressure outlet. The turbulence model used is the Realizable k-ε model. The time step is 0.01 s, and 200 steps are taken as one calculation. The total computational domain is a rectangular box, with a total length of 3 L, a width of 4 W, and a height of 6 H. The external flow field is automatically divided into tetrahedral meshes, and three prism layers are added at the interface with the shell surface to improve the calculation and analysis accuracy. As the point of action of the hind legs (hip joint), the point of action of the tail (tail joint), and the force point of the shell impaction are fixed with respect to the body coordinate system, the disturbance torque $M_D$ is independent of the attitude angle, calculation process is shown in Figure 5.

The recovery moment $M_R$ of the beaver-like robot is composed of the robot gravity $G$ and the buoyancy $F_f$. It can be expressed as follows:

$$M_R = R_\Omega(\varphi, \theta, \gamma) \cdot G \cdot C_b + R_\Omega(\varphi, \theta, \gamma) \cdot F_f \cdot B_b \quad (2)$$

$R_\Omega(\phi, \theta, \gamma)$ is the transformation matrix of the attitude angle. In the simulation calculation, the attitude angle is obtained by Adams simulation, and the expression of $R_\Omega(\phi, \theta, \gamma)$ is
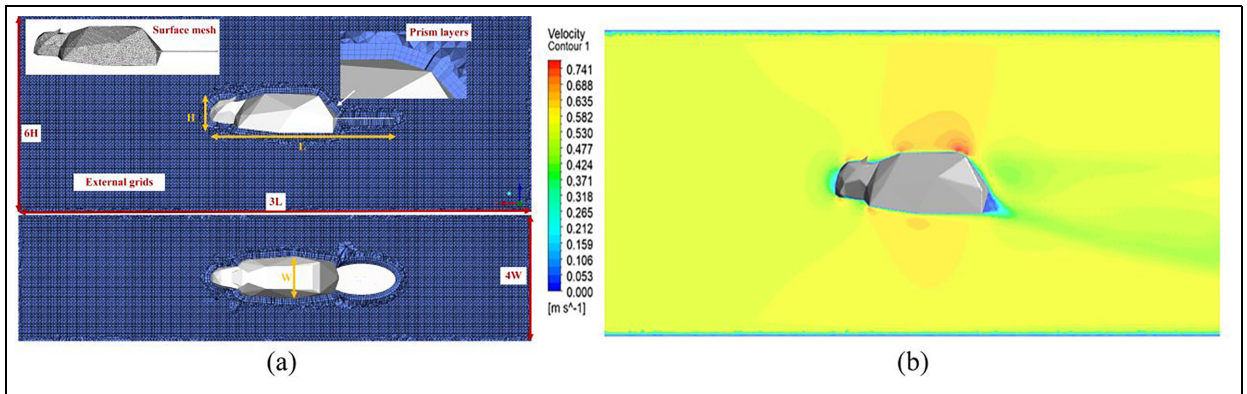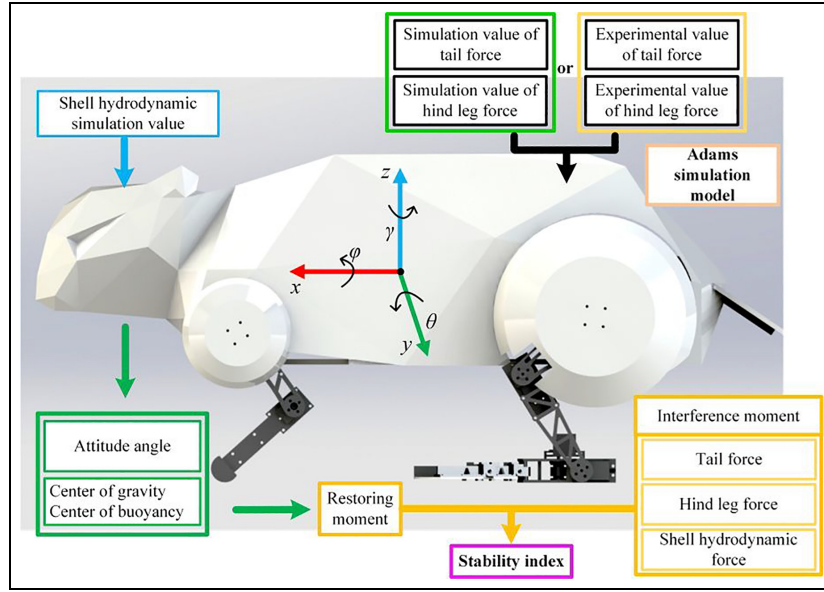


**Figure 4.** Shell fluent simulation: (a) outer shell field meshing, (b) outflow field velocity cloud image.

**Figure 5.** Calculation of body coordinate system, attitude angle, and stability index of the beaver-like robot.

$$R_\Omega(\varphi,\theta,\gamma) =$$
$$\begin{bmatrix} \cos\theta\cos\gamma & -\cos\theta\sin\gamma & \sin\theta \\ \sin\varphi\sin\theta\cos\gamma + \cos\varphi\sin\gamma & -\sin\varphi\sin\theta\sin\gamma + \cos\varphi\cos\gamma & -\sin\varphi\cos\theta \\ -\cos\varphi\sin\theta\cos\gamma + \sin\varphi\sin\gamma & \cos\varphi\sin\theta\sin\gamma + \sin\varphi\cos\gamma & \cos\varphi\cos\theta \end{bmatrix}$$
(3)

Among them, the overall gravity center coordinates $C_b$ and floating center coordinates $B_b$ change with the movement of the leg mechanism and tail when the beaver-like robot is in motion. The gravity center coordinates and floating center coordinates are thus expressed as follows. Their parameters are shown in Table 2.

$$C_b = \frac{\sum_{j=0}^{n} m_j{}^b C_j}{m} \Leftrightarrow \begin{cases} x_g = \dfrac{\sum_{j=0}^{n} m_j{}^b x_{cj}}{\sum_{j=0}^{n} m_j} = \dfrac{\sum_{j=0}^{n} m_j{}^b x_{cj}}{m} \\[3ex] y_g = \dfrac{\sum_{j=0}^{n} m_j{}^b y_{cj}}{\sum_{j=0}^{n} m_j} = \dfrac{\sum_{j=0}^{n} m_j{}^b y_{cj}}{m} \\[3ex] z_g = \dfrac{\sum_{j=0}^{n} m_j{}^b z_{cj}}{\sum_{j=0}^{n} m_j} = \dfrac{\sum_{j=0}^{n} m_j{}^b z_{cj}}{m} \end{cases}$$
(4)

$$B_b = \frac{\sum_{j=0}^{n} V_j{}^b B_j}{V} \Leftrightarrow \begin{cases} x_f = \dfrac{\sum_{j=0}^{n} V_j{}^b x_{bj}}{\sum_{j=0}^{n} V_j} = \dfrac{\sum_{j=0}^{n} V_j{}^b x_{bj}}{V} \\[3ex] y_f = \dfrac{\sum_{j=0}^{n} V_j{}^b y_{bj}}{\sum_{j=0}^{n} V_j} = \dfrac{\sum_{j=0}^{n} V_j{}^b y_{bj}}{V} \\[3ex] z_f = \dfrac{\sum_{j=0}^{n} V_j{}^b z_{bj}}{\sum_{j=0}^{n} V_j} = \dfrac{\sum_{j=0}^{n} V_j{}^b z_{bj}}{V} \end{cases}$$
(5)

*Swimming stability margin of the beaver-like robot*

On the basis of the derivation in the previous section, the swimming stability index of the beaver-like robot can be expressed as follows:

$$M_D/M_R = \frac{F_h \cdot s_h + F_t \cdot s_t + F_s \cdot s_m}{R_\Omega(\varphi,\theta,\gamma) \cdot G \cdot C_b + R_\Omega(\varphi,\theta,\gamma) \cdot F_f \cdot B_b}$$
(6)

**Table 2.** Expression parameters of centers of gravity and buoyancy of the beaver-like robot.

| Parts | J | Center of gravity | Center of buoyancy | Weight | Volume |
|---|---|---|---|---|---|
| Trunk | Trunk (0) | $^bC_j = \begin{bmatrix} ^b x_{cj} \\ ^b y_{cj} \\ ^b z_{cj} \end{bmatrix}$ | $^bB_j = \begin{bmatrix} ^b x_{bj} \\ ^b y_{bj} \\ ^b z_{bj} \end{bmatrix}$ | $m_0$ | $V_0$ |
| Hind legs | Hip joint (1) | | | $m_1$ | $V_1$ |
| | Knee joint (2) | | | $m_2$ | $V_2$ |
| | Ankle joint (3) | | | $m_3$ | $V_3$ |
| | Knuckle 1 (4) | | | $m_4$ | $V_4$ |
| | Knuckle 2 (5) | | | $m_5$ | $V_5$ |
| Tail | Tail joint (6) | | | $m_6$ | $V_6$ |

It can only reflect whether the robot is stable or not and cannot measure the stability margin of the robot in the dynamic motion state. Stability margin refers to the margin of a certain quantity change away from the instability of the system, which is of great significance for evaluating the ability of the robot to maintain stability. In this study, $S$ is used as a measure of the swimming stability margin of the beaver-like robot. It is denoted by

$$
\begin{aligned}
S &= 1 - M_D/M_R \\
&= 1 - \frac{F_h \cdot s_h + F_t \cdot s_t + F_s \cdot s_m}{R_\Omega(\varphi, \theta, \gamma) \cdot G \cdot C_b + R_\Omega(\varphi, \theta, \gamma) \cdot F_f \cdot B_b}
\end{aligned} \tag{7}
$$

Through the research on the stability margin of the alternating and synchronous gaits under the bionic, increasing, and reducing gaits, the stability margin of the robot under different gaits and motion amplitudes is obtained. The obtained values provide reference for the subsequent improvement of the motion performance of the robot.

## Simulation and experiment of swimming stability criteria for beaver-like robot

### Adams–Matlab co-simulation

The Adams–Matlab co-simulation is used to calculate the swimming stability index of the beaver-like robot, the calculation process is shown in Figure 6. Basing on the research on the rigid-fluid fusion dynamics of the hind legs and the segmental dynamics of the tail of the beaver-like robot and considering the simulation and experimental results of the propulsion and lift forces of the hind legs and tail to the torso, we respectively integrated the simulation and experimental values under different gaits into the underwater motion simulation model of the beaver-like robot in Adams. The overall flow resistance of the robot obtained from ANSYS Fluent simulation was added to simulate the underwater swimming of the robot. The change in the attitude angle of the robot while swimming was calculated through Adams simulation. The attitude angle information was then imported into Matlab and jointly



**Figure 6.** Stability index calculation process.

calculated with the stability index model to obtain the stability margin $S$.

### Adams simulation

The virtual prototype model of underwater robot is established in SolidWorks, and the virtual prototype model of underwater robot is established in ADAMS. The parts without relative motion in the model are summed by Boolean, and the parts without influence on the movement of the robot are removed, which reduces the complexity of the processing and the uncertainty of the model simulation. The forces exerted by the hind legs and tail on the trunk of the robot are added to the hip joint and tail joint. The motion of the gait corresponding to the hind legs and tail is adjusted to replicate the real motion state. The water flow resistance model under different speeds obtained from the Fluent simulation is applied to the shell. Thus, the attitude angle information of the beaver-like robot is obtained.

To achieve a better control effect, this study compares the stability index of different gaits with the stability index of different motion functions under the same gait. It then verifies the stability difference between gaits and the influence of different motion functions on stability, allaying the foundation for the subsequent stable motion control and optimization of the robot. Figures 7 and 10 show the changes in motion under the bionic alternating gait and those under the bionic synchronous gait, respectively. In the bionic alternating gait, the hind legs swing alternately, the tail swing is larger, and the body fluctuation is smaller. In the bionic synchronous gait, the hind legs of the robot maintain the same swing position, generating more power. Although the tail swing is smaller, it stabilizes the trunk. Nonetheless, the body fluctuates greatly during movement. Figures 8 and 9 show the increased and reduced gaits under alternating gait, respectively. The results of Adams simulation reveal that the pitch angle and roll angle of the robot with increased gait vary greatly, and the overall stability of the robot is poor. Although the robot with reduced gait has good overall stability, the movement is relatively slow. Figures 11 and 12 show the increased and reduced gaits under synchronous gait. The increased gait under synchronous gait has the same characteristics as that under alternating gait, but the stability is worse.

### Experiment

The experiment was carried out in a transparent water tank with the length × width × height of $2\,m \times 1\,m \times 1.2\,m$, and the motion of the robot prototype was captured by a high-definition camera. Figures 13 and 14 respectively show the motion process of the flippers in alternating stroke and synchronous stroke modes. In alternating strokes, the two hind legs achieve the body's progress through alternating strokes. In one movement
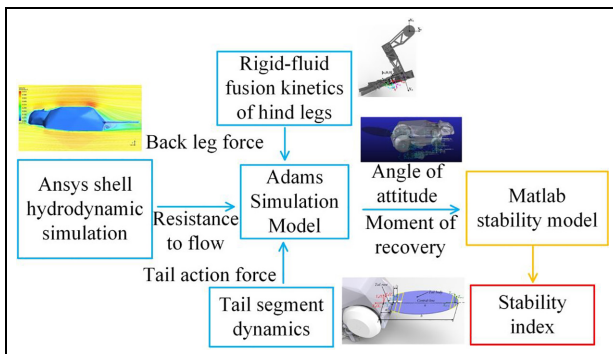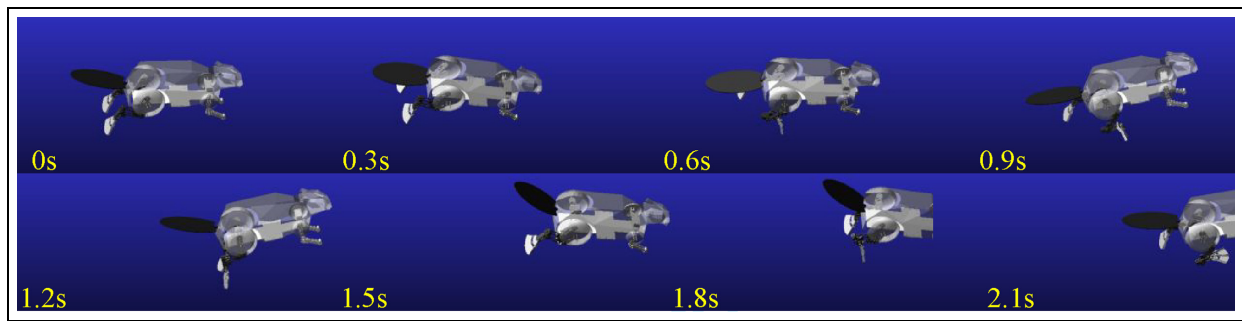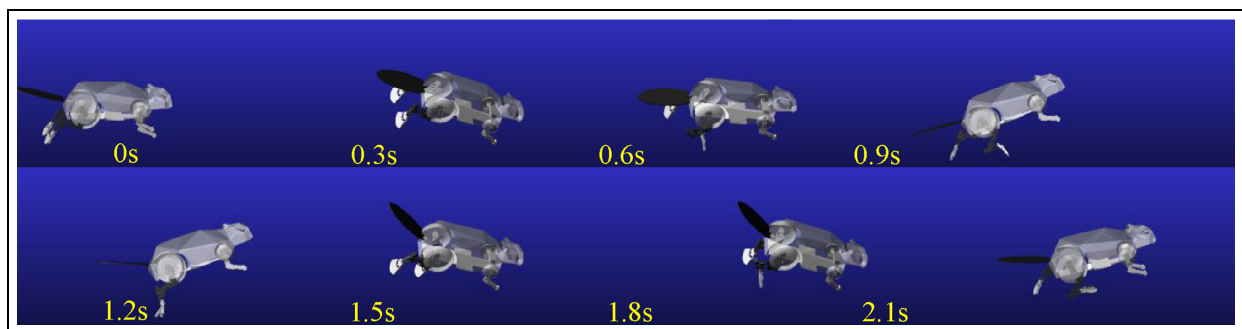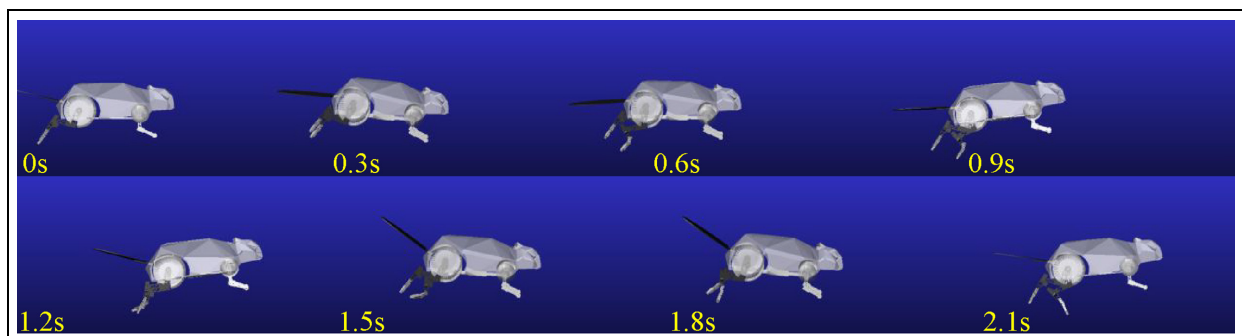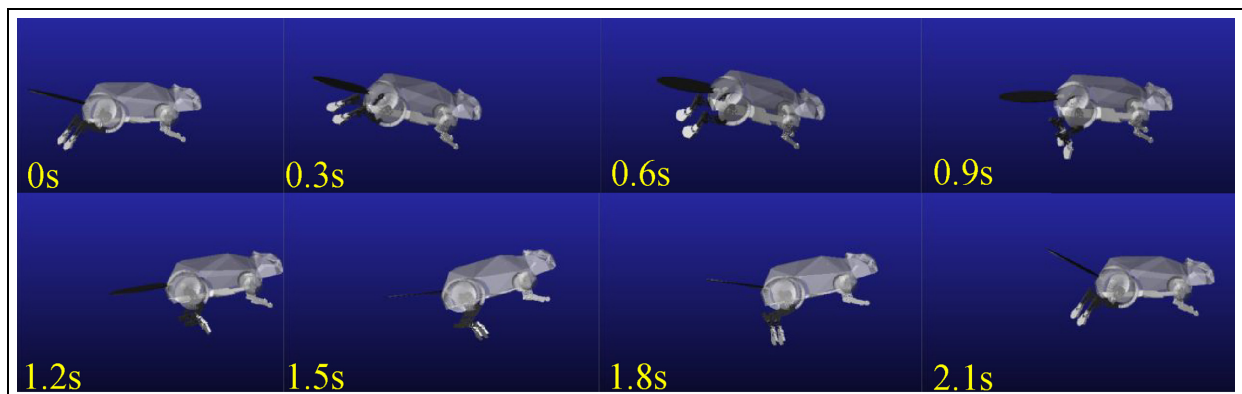
**Figure 7.** Changes in motion under a bionic alternating gait.



**Figure 8.** Changes in motion under incremental alternating gait.
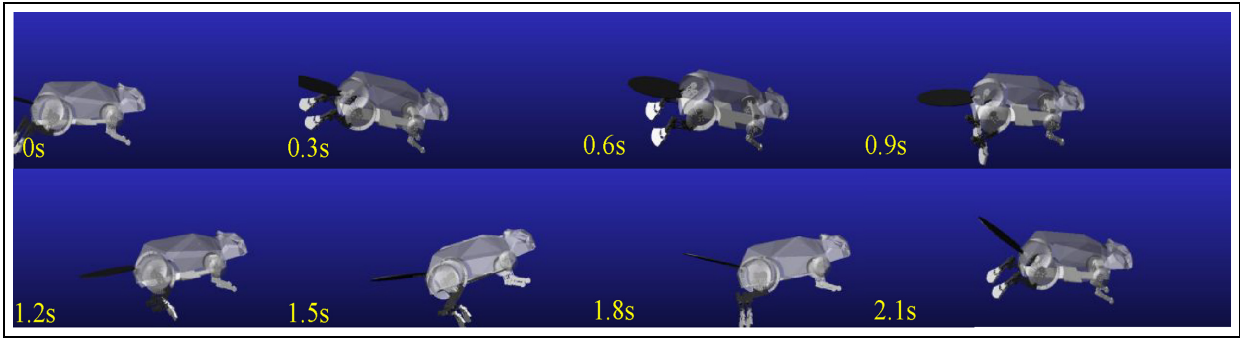


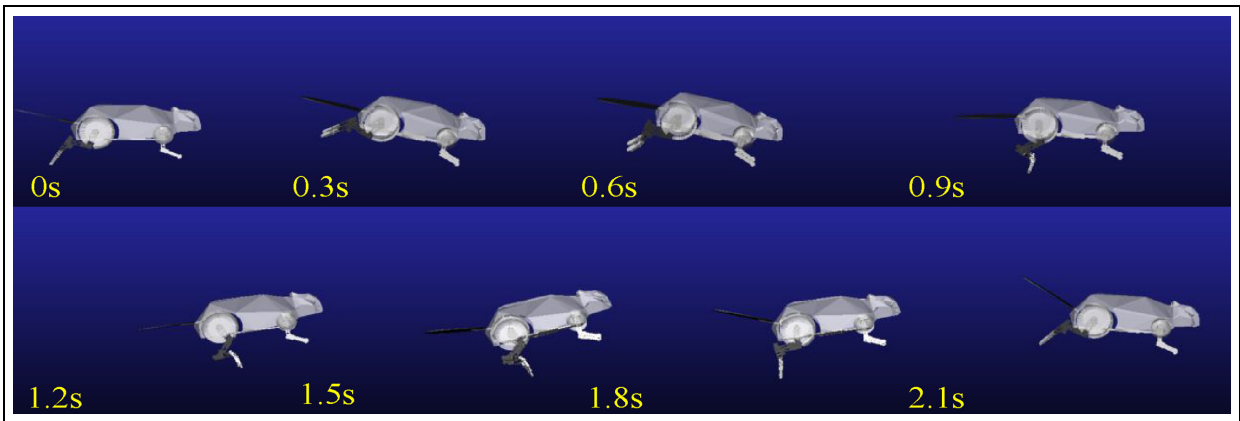**Figure 9.** Changes in motion under reduced-amplitude alternating gait.



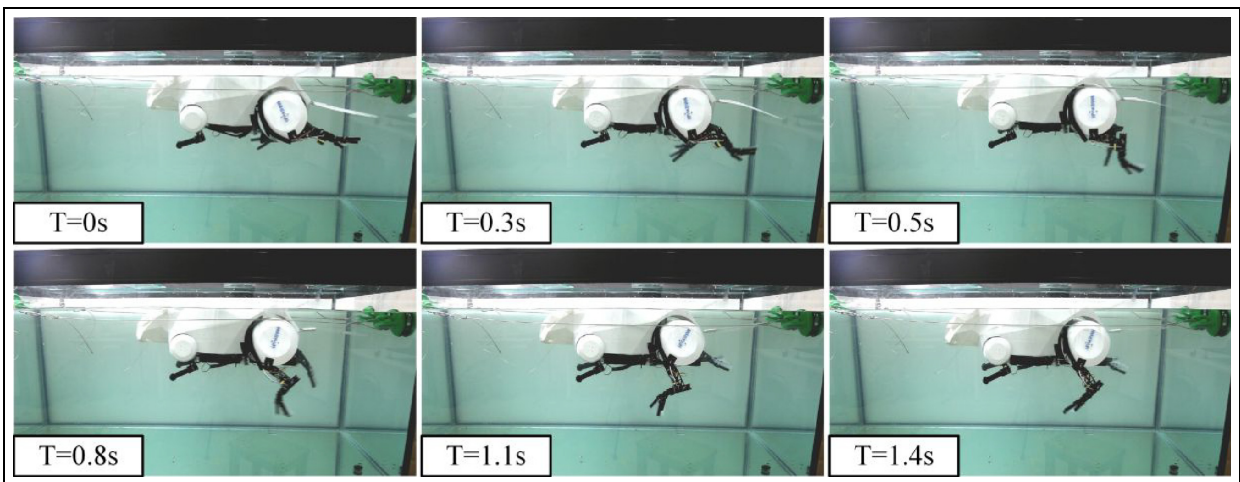**Figure 10.** Changes in motion under bionic synchronized gait.

**Figure 11.** Changes in motion under reduced-amplitude synchronized gait.



**Figure 12.** Changes in motion under synchronized gait.



**Figure 13.** Alternating gait.

cycle, the two flippers alternately provide propulsion, so that the body can continue to move, and the movement process is relatively stable. In the recovery phase, the fins bend and contract to reduce the area of the oncoming stream, thereby reducing the resistance of the flow. In synchronous stroke, the two hind legs move synchronously to achieve the body's forward movement. In one movement cycle, the two flippers simultaneously provide propulsion and withstand the water resistance at the same time. The propulsion force is discontinuous, and the movement process is not smooth, but the movement is explosive. In the alternating flipper stroke, the two flippers produce propulsion force, which causes the force imbalance in the horizontal plane of the robot, and the body moves left and right in the horizontal plane. In the synchronous paddling of the flippers, the two flippers are paddling at the same time, and the force of the robot in the
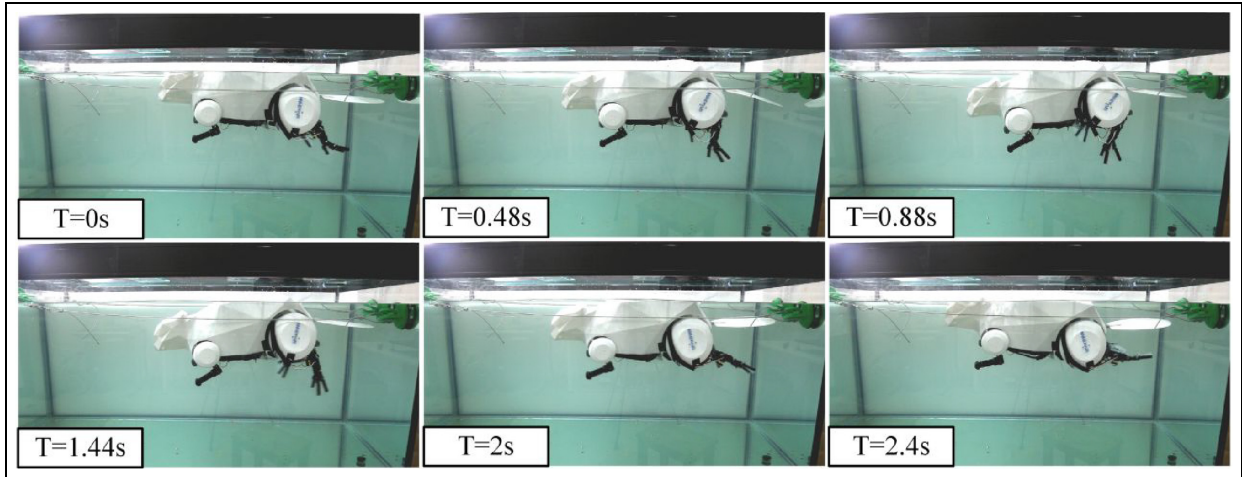
**Figure 14.** Synchronized gait.

horizontal plane is more uniform, which avoids its shaking in the horizontal plane, but increases the force in the vertical direction, resulting in the pitching of the robot in the movement.
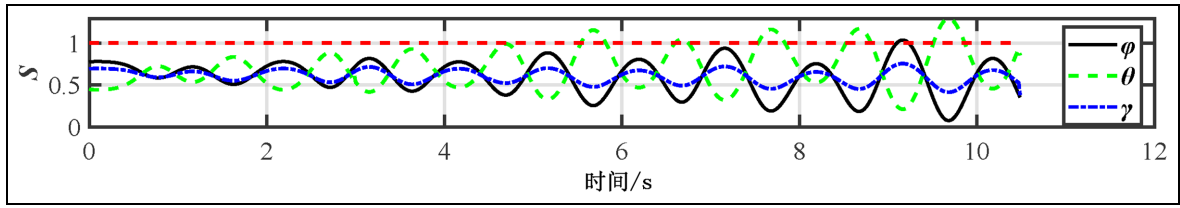
### Results of stability index calculation

By modeling and calculating the bionic, increasing, and decreasing motion functions under the two types of straight gait, the bionic gait is extracted from the biological motion posture analysis to obtain the skeletal posture and motion trajectory of the biological motion. Subsequently, we determined the motion function of the hind leg and tail. The increase and decrease motion function is the gait obtained by increasing and decreasing the amplitude value based on the bionic gait. The difference between alternating and synchronous gaits lies in the phase difference between the two hind legs in alternating gait, which makes the two hind legs produce propulsion force alternately. In synchronous gait, no phase difference exists between the two hind legs, and the propulsion force is generated simultaneously.

*Results of the alternating gait stability index.* Figures 15–20 show the stability index calculation results of simulation values and experimental values under bionic, increasing and decreasing alternating gait respectively. From the figure, we can obtain the following information:

(1) The changes of the three indicators $S_\phi$, $S_\theta$, and $S_\gamma$ show a sinusoidal change state, and the change amplitude of $S_\phi$ and $S_\theta$ has an obvious trend of increasing with time.

(2) The three motion functions of $S_\gamma$ in alternating gait are all less than 1, and the simulation results are maintained at 0.65, 0.6, 0.55 respectively, and the experimental results are maintained at 0.48,

0.51, 0.50 respectively. Therefore, the robot has high stability in yaw angle $\gamma$.

(3) $S_\theta$ starts to be greater than 1 after 5.8 s in the bionic gait, and the maximum value of the simulation results is 1.18, and the maximum value of the experimental results is 1.09. In the increasing gait, it starts to be greater than 1 after 4.3 s, and the maximum simulation results reach 1.48, and the maximum experimental results reach 1.32. Under the reduced gait, the simulation results and experimental results are almost less than 1, and the stability is good.

(4) The simulation value and experimental value of $S_\phi$ under bionic gait are up to 1.02 and 0.91, respectively. Under the reduced gait, the simulation calculated value, and the experimental calculated value are up to 1.21 and 1.08 respectively. Under the increasing gait, the maximum value of simulation calculation and experimental calculation reaches 1.21, 1.08 respectively, and starts to be greater than 1 after 4.7 s. The maximum value of simulation calculation reaches 1.16, and the maximum value of experimental calculation reaches 1.06.

(5) There is almost no phase difference between the calculation results of the experimental value and the simulation value, and the calculation curve of the experimental value is not smooth, and there is a certain deviation, which may be caused by the assembly error and sensor measurement error in the experiment; And the experimental results are lower than the simulation results.
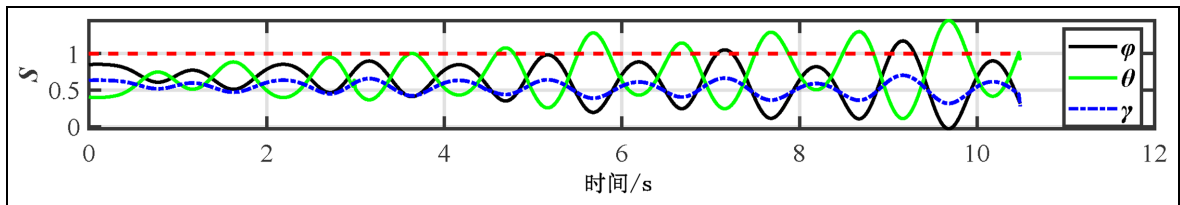
*Results of stability indices in synchronized gait.* Figures 21–26 show the stability index calculation results of simulation values and experimental values under bionic, increasing
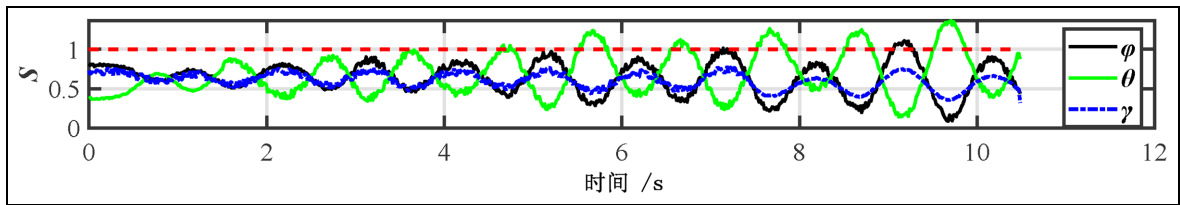
**Figure 15.** Stability index under bionic alternating gait (simulation results).
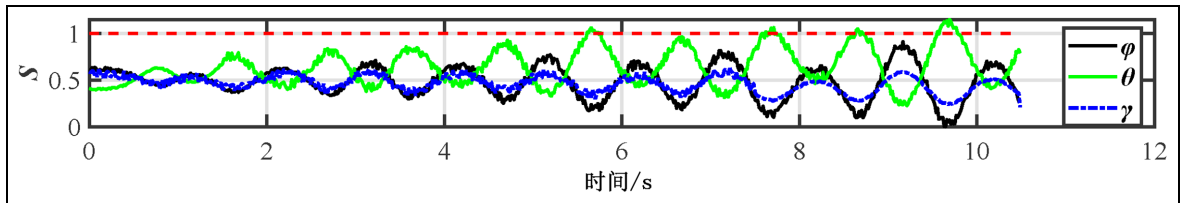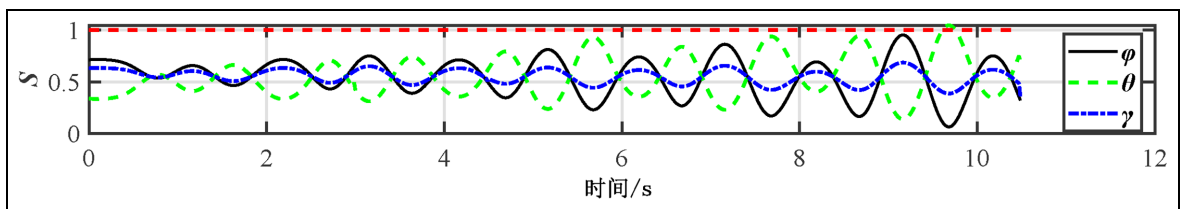


**Figure 16.** Stability index under bionic alternating gait (experimental results).
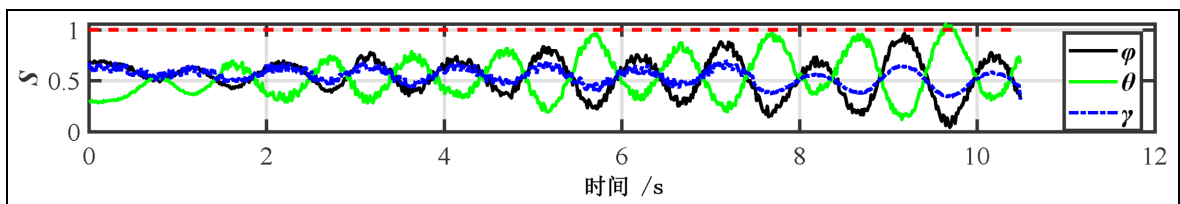


**Figure 17.** Stability index under increasing alternating gait (simulation results).
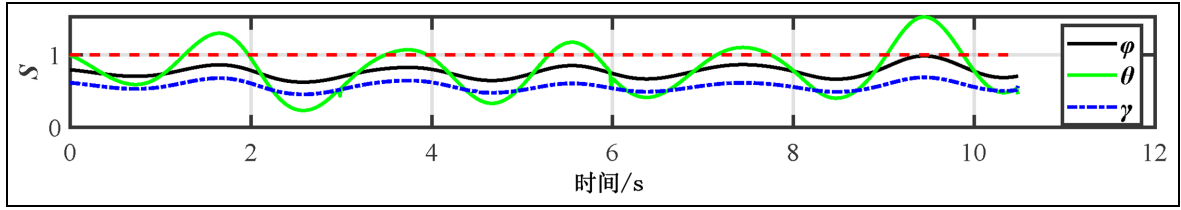


**Figure 18.** Stability index under increasing alternating gait (experimental results).
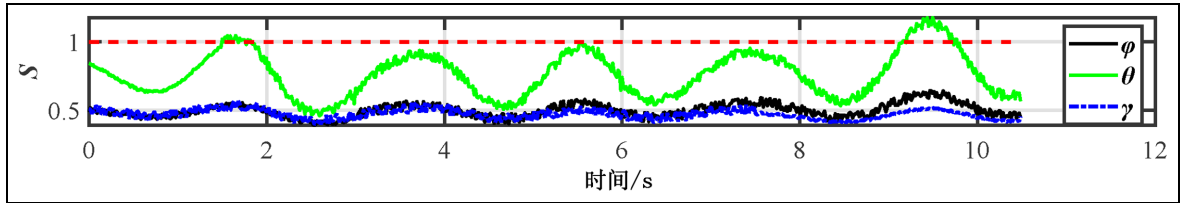


**Figure 19.** Stability index under reduced alternating gait (simulation results).
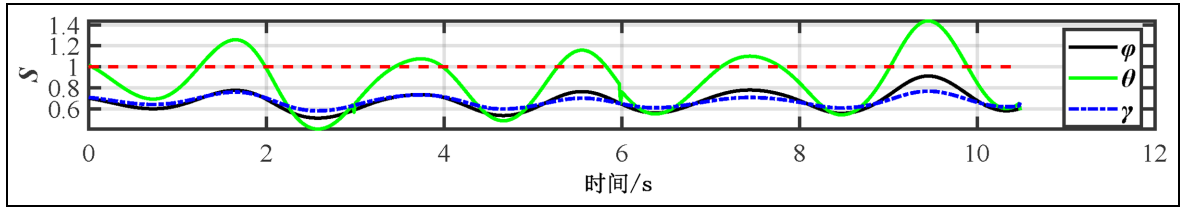


**Figure 20.** Stability index under reduced amplitude alternating gait (experimental results).
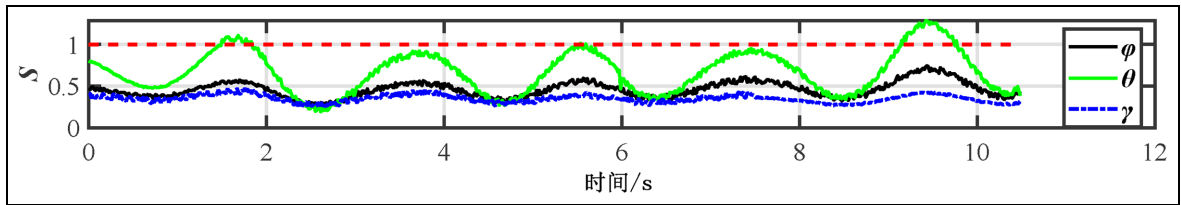
**Figure 21.** Stability index under bionic synchronous gait (simulation results).
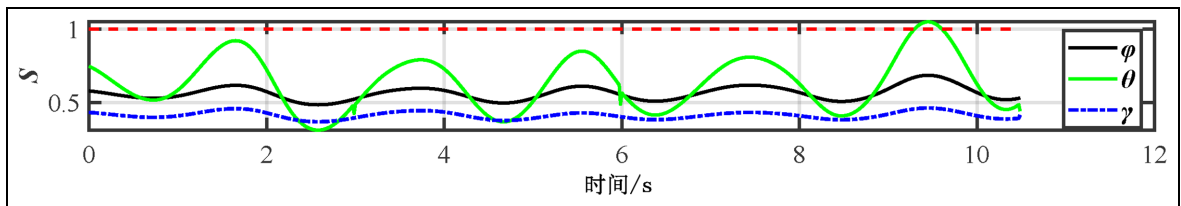


**Figure 22.** Stability index under bionic synchronous gait (experimental results).



**Figure 23.** Stability index under incrementally synchronized gait (simulation results).
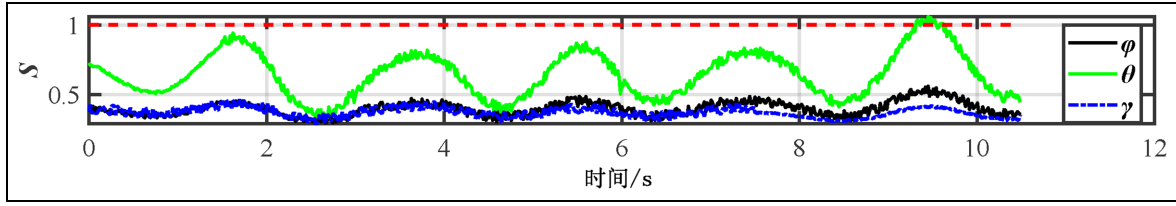


**Figure 24.** Stability index under increasing gait synchronization (experimental results).



**Figure 25.** Stability index under reduced amplitude synchronous gait (simulation results).

and decreasing synchronized gait respectively. From the figures, we can obtain the following information:

(1) The changes of the three indicators $S_\phi$, $S_\theta$, and $S_\gamma$ show sinusoidal changes in the simulation results and experimental results, and the change period is longer than that of the alternating gait. The change amplitude of $S_\phi$ and $S_\gamma$ is small, but the change value of $S_\theta$ is large.

(2) The three motion functions of $S_\phi$ and $S_\gamma$ in synchronous gait are all less than 1, and the robot has high stability in roll angle $\phi$ and yaw angle $\gamma$ under synchronous gait. Compared with the alternating gait, the synchronous gait has better stability in the roll angle, but worse stability in the pitch angle.

(3) $S_\theta$ is greater than 1 in many cycles of bionic gait, and the maximum excess value of the simulation

**Figure 26.** Stability index under reduced amplitude synchronous gait (experimental results).

**Table 3.** Maximum value of attitude angle stability index.

| Gait | $S_{\phi\_m}$ | | $S_{\theta\_m}$ | | $S_{\gamma\_m}$ | |
|---|---|---|---|---|---|---|
| | Experiment | Simulation | Experiment | Simulation | Experiment | Simulation |
| Bionic alternating gait | 1.02 | 0.93 | 0.52 | 0.48 | 0.52 | 0.50 |
| Augmented alternating gait | 1.18 | 1.23 | 1.39 | 1.41 | 0.42 | 0.38 |
| Reduced alternating gait | 0.82 | 1.08 | 0.62 | 0.58 | 0.58 | 0.54 |
| Bionic synchronous gait | 0.36 | 0.33 | 1.2 | 1.23 | 0.42 | 0.40 |
| Augmented synchronous gait | 0.42 | 0.37 | 1.29 | 1.51 | 0.32 | 0.38 |
| Reduced synchronous gait | 0.52 | 0.55 | 1.10 | 1.09 | 0.68 | 0.64 |

value is 0.29, and the maximum excess value of the experimental value is 0.13. Under the increasing gait, the five change cycles are all greater than 1, and the maximum excess value of the simulation value calculation results is 0.42, and the maximum excess value of the experimental value calculation results is 0.22. In the reduced gait, almost all of them are less than 1, and the stability is good.

Table 3 shows the maximum value of stability index of each attitude angle calculated. Combined with the calculation curve, it can be seen that under the same gait, the stability margin decreases with the increase of amplitude, the amplitude reduction gait is the most stable, the bionic gait is relatively stable, and the stability of the increase gait is the worst. In the straight motion, there is instability in the pitch angle and roll angle. The stability margin of synchronous gait in yaw angle and roll angle is larger than that of alternating gait, but the stability margin of alternating gait in pitch angle is larger.

## Conclusions and future work

This study proposes a stability index and evaluation method on the basis of the determination of the couple moment for assessing the motion stability of the beaver-like robot. The results of stability index calculation align with the information obtained from the diagrams illustrating the changes in the motion in Adams simulation. Both prove that the stability of the beaver-like robot in the roll angle and yaw angle is worse under alternating gait, whereas the stability in the pitch angle is worse under synchronous gait. The increase of

the motion amplitude of the propulsion structure (hind legs and tail) reduces the motion stability of the robot. However, the results of the Adams simulation indicate that the velocity is reduced when the amplitude is reduced. From the above results, it can be seen that compared with the traditional stability analysis methods, the stability analysis method proposed in this paper not only considers the stability of the robot under static conditions, but also includes the recovery ability of the robot in the dynamic process, because the recovery torque is often closely related to the dynamic characteristics of the robot, such as mass distribution and propulsion mode. This dynamic adaptability makes the metric more advantageous when evaluating the stability of robots in complex underwater environments.

In future research, we will design a more efficient controller by iteratively optimizing the control parameters with the stability index as the optimization target. By constantly adjusting the control parameters, the motion amplitude of each propulsion structure is optimized to make the robot maintain a certain stability and achieve the required motion performance. In addition, we will continue to explore the interaction between the tail and other robot components to optimize the mechanical and dynamic properties of the propulsion structure, so as to improve the stability and motion performance of the robot, making the robot have better flexibility and reliability in various complex environments and tasks.

### Declaration of conflicting interests

The author(s) declared no potential conflicts of interest with respect to the research, authorship, and/or publication of this article.

## ORCID iD

Gang Chen [iD] https://orcid.org/0000-0003-3926-9149

## References

1. Chen G, Xu Y, Yang C, et al. Design and control of a novel bionic mantis shrimp robot. *IEEE/ASME Trans Mechatron* 2023; 28: 3376–3385.
2. Yan Z, Yang H, Zhang W, et al. Robust nonlinear model predictive control of a bionic underwater robot with external disturbances. *Ocean Eng* 2022; 253: 111310.
3. Chen G, Han Y, Li Y, et al. Autonomous gait switching method and experiments of a hexapod walking robot for Mars environment with multiple terrains. *Intell Serv Robot* 2024; 17: 1–21.
4. Cong Y, Gu C, Zhang T, et al. Underwater robot sensing technology: a survey. *Fundam Res* 2021; 1(3): 337–345.
5. Xu H, Pan C, Xie H, et al. Dynamics modeling and simulation of a bionic swim bladder system in underwater robotics. *J Bionic Eng* 2008; 5(1): 66–71.
6. Chen G, Xu Y, Yang X, et al. Target tracking control of a bionic mantis shrimp robot with closed-loop central pattern generators. *Ocean Eng* 2024; 297: 116963.
7. Costa D, Palmieri G, Palpacelli M, et al. Design of a bio-inspired autonomous underwater robot. *J Intell Robot Syst* 2018; 91: 181–192.
8. Zhou H, Hu T, Xie H, et al. Computational and experimental study on dynamic behavior of underwater robots propelled by bionic undulating fins. *Sci China Technol Sci* 2010; 53: 2966–2971.
9. Rosell F, Bozser O, Collen P, et al. Ecological impact of beavers castor fiber and castor canadensis and their ability to modify ecosystems. *Mamm Rev* 2005; 35(3–4): 248–276.
10. Polvi LE and Wohl E. The beaver meadow complex revisited–the role of beavers in post-glacial floodplain development. *Earth Surf Process Landf* 2012; 37(3): 332–346.
11. Siemer WF, Jonker SA, Decker DJ, et al. Toward an understanding of beaver management as human and beaver densities increase. *Hum-Wildl Interact* 2013; 7(1): 114–131.
12. Chen G, Lu Y, Yang X, et al. Reinforcement learning control for the swimming motions of a beaver-like, single-legged robot based on biological inspiration. *Robot Auton Syst* 2022; 154: 104116.
13. Chen G, Peng W, Wang Z, et al. Modeling of swimming posture dynamics for a beaver-like robot. *Ocean Eng* 2023; 279: 114550.
14. Chen G, Xu Y, Yang C, et al. Dynamic modeling and experimental analysis of a novel bionic mantis shrimp robot. *J Field Robot* 2024; 1–17.
15. Miller SC. Profiling sulfonate ester stability: identification of complementary protecting groups for sulfonates. *J Org Chem* 2010; 75(13): 4632–4635.
16. Kornuta T and Zieliński C. Robot control system design exemplified by multi-camera visual servoing. *J Intell Robot Syst* 2015; 77: 499–523.
17. Tsumugiwa T, Fuchikami Y, Kamiyoshi A, et al. Stability analysis for impedance control of robot in human-robot cooperative task system. *J Adv Mech Des Syst Manuf* 2007; 1(1): 113–121.
18. Antonelli G. Stability analysis for prioritized closed-loop inverse kinematic algorithms for redundant robotic systems. *IEEE Trans Robot* 2009; 25(5): 985–994.
19. Nava G, Romano F, Nori F, et al. Stability analysis and design of momentum-based controllers for humanoid robots. In: *2016 IEEE/RSJ international conference on intelligent robots and systems (IROS)*, Daejeon, Korea (South). IEEE, 2016, pp.680–687.
20. Mejri S, Gagnol V, Le T, et al. Dynamic characterization of machining robot and stability analysis. *Int J Adv Manuf Technol* 2016; 82: 351–359.
21. Seo K, Cho S, Kim T, et al. Design and stability analysis of a novel wall-climbing robotic platform (ROPE RIDE). *Mech Mach Theory* 2013; 70: 189–208.
22. Zake Z, Chaumette F, Pedemonte N, et al. Vision-based control and stability analysis of a cable-driven parallel robot. *IEEE Robot Autom Lett* 2019; 4(2): 1029–1036.
23. Liljeback P, Pettersen KY, Stavdahl Ø, et al. Controllability and stability analysis of planar snake robot locomotion. *IEEE Trans Autom Control* 2010; 56(6): 1365–1380.
24. Wen JT and Murphy S. Stability analysis of position and force control for robot arms. *IEEE Trans Autom Control* 1991; 36(3): 365–371.
25. Liang P, Gao X, Zhang Q, et al. Design and stability analysis of a wall-climbing robot using propulsive force of propeller. *Symmetry* 2020; 13(1): 37.
26. Papaloizou J and Pringle JE. The dynamical stability of differentially rotating discs with constant specific angular momentum. *Mon Not R Astron Soc* 1984; 208(4): 721–750.
27. Papadopoulos E and Rey DA. The force-angle measure of tipover stability margin for mobile manipulators. *Veh Syst Dyn* 2000; 33(1): 29–48.
28. Migdalovici M, Vlădăreanu L, Baran D, et al. Stability analysis of the walking robots motion. *Procedia Comput Sci* 2015; 65: 233–240.
29. Kuznetsov NV and Leonov GA. Lyapunov quantities, limit cycles and strange behavior of trajectories in two-dimensional quadratic systems. *J Vibroeng* 2008; 10(4): 460–467.
30. Michel AN. Recent trends in the stability analysis of hybrid dynamical systems. *IEEE Trans Circuits Syst I Fundam Theory Appl* 1999; 46(1): 120–134.
31. Lakshmikantham V, Leela S and Martynyuk AA. *Stability analysis of nonlinear systems*. New York: Springer, 1989.

32. Fareh R, Khadraoui S, Abdallah MY, et al. Active disturbance rejection control for robotic systems: a review. *Mechatronics* 2021; 80: 102671.

33. Jiang B, Karimi HR, Yang S, et al. Observer-based adaptive sliding mode control for nonlinear stochastic Markov jump systems via T–S fuzzy modeling: applications to robot arm model. *IEEE Trans Ind Electron* 2020; 68(1): 466–477.

34. Butler DR and Malanson GP. The geomorphic influences of beaver dams and failures of beaver dams. *Geomorphology* 2005; 71(1–2): 48–60.

35. Brazier RE, Puttock A, Graham HA, et al. Beaver: nature's ecosystem engineers. *Wiley Interdiscip Rev: Water* 2021; 8(1): e1494.

36. Howard RJ and Larson JS. A stream habitat classification system for beaver. *J Wildl Manag* 1985; 49: 19–25.

37. Westbrook CJ, Cooper DJ and Baker BW. Beaver assisted river valley formation. *River Res Appl* 2011; 27(2): 247–256.

38. Chen G, Xu Y, Wang Z, et al. Dynamic tail modeling and motion analysis of a beaver-like robot. *Nonlinear Dyn* 2024; 112: 6859–6875.